Voltage Pulses Change Neural Interface Properties and Improve Unit Recordings With Chronically Implanted Microelectrodes

Kevin J. Otto*, *Member, IEEE*, Matthew D. Johnson, *Member, IEEE*, and Daryl R. Kipke, *Member, IEEE*

***Abstract*—Current neuroprosthetic systems based on electrophysiological recording have an extended, yet finite working lifetime. Some posited lifetime-extension solutions involve improving device biocompatibility or suppressing host immune responses. Our objective was to test an alternative solution comprised of applying a voltage pulse to a microelectrode site, herein termed "rejuvenation." Previously, investigators have reported preliminary electrophysiological results by utilizing a similar voltage pulse. In this study we sought to further explore this phenomenon via two methods: 1) electrophysiology; 2) an equivalent circuit model applied to impedance spectroscopy data. The experiments were conducted via chronically implanted silicon-substrate iridium microelectrode arrays in the rat cortex. Rejuvenation voltages resulted in increased unit recording signal-to-noise ratios ($10\% \pm 2\%$), with a maximal increase of 195% from 3.74 to 11.02. Rejuvenation also reduced the electrode site impedances at 1 kHz ($67\% \pm 2\%$). Neither the impedance nor recording properties of the electrodes changed on neighboring microelectrode sites that were not rejuvenated. In the equivalent circuit model, we found a transient increase in conductivity, the majority of which corresponded to a decrease in the tissue resistance component ($44\% \pm 7\%$). These findings suggest that rejuvenation may be an intervention strategy to prolong the functional lifetime of chronically implanted microelectrodes.**

***Index Terms*—Brain-machine interface, chronic recording, iridium, neuroprosthesis, silicon.**

I. Introduction

LONG-TERM multichannel extracellular recordings of neural responses have potential in both research and neuroprosthetic applications. Several research groups have developed devices that are capable of recording from dozens of neurons for time periods of weeks to months [1]–[5]. These devices have various success rates, ranging from 54%–80% of the sites recording single and multi-unit activity over periods of 3–24 weeks [6]–[9]. Reactive tissue responses have been implicated as detractors to long-term recording performance [10]–[13].

Manuscript received October 12, 2004; revised May 1, 2005. This work was supported in part by the Defense Advanced Research Projects Agency under Grant DARPA: N66001-02-C-8059, in part by the Center for Neural Communication Technology under Grant P41-EB00230, and in part by the Engineering Research Centers program of the National Science Foundation (NSF) under Award EEC-9986866. *Asterisk indicates corresponding author.*

*K. J. Otto is with the Kresge Hearing Research Institute, University of Michigan, Ann Arbor, MI 48109 USA (e-mail: kjotto@umich.edu).

M. D. Johnson and D. R. Kipke are with the Biomedical Engineering Department, University of Michigan, Ann Arbor, MI 48109 USA (e-mail: mdjzz@umich.edu; dkipke@umich.edu).

Digital Object Identifier 10.1109/TBME.2005.862530

Reports have shown an early and sustained immune response to penetrating injury of the brain [11], [12]. This response can result in a compact sheath of glial cells and connective tissue around chronically implanted microelectrodes, thereby functionally isolating them from the brain. Thus, minimizing the tissue reaction at microelectrode sites is important for extending the functional longevity of chronically implanted microelectrode arrays. Several methods have been reported in an effort to hinder one aspect of the reaction, the glial response, thereby improving the neural interface with the recording devices. These methods include: optimizing the shape of the tip and shaft of the implants [14], optimizing insertion [15], coating the electrodes with biomolecules [16], systemic or local delivery of anti-inflammatory drugs [17], and constructing the devices from alternative device substrates [18]. Alternatively, passing current through an iridium neural microelectrode *in vivo* has been shown to cause a reduced 1-kHz site impedance and improvement in unit recordings [19], [20]. However, the underlying mechanisms for this improvement in recordings and drop in impedance are not fully known.

In the present study, we investigated how voltage pulses (rejuvenation) affect the electrophysiological and electrochemical properties of chronically implanted iridium microelectrodes. We utilized extracellular recordings as well as complex impedance spectroscopy to evaluate the electrode interface and the surrounding neural tissue through an equivalent circuit model.

II. Methods

A. Experimental Procedures and Microelectrode Arrays

Eight male Sprague-Dawley rats (250–300 g) were chronically implanted with silicon-substrate microelectrode arrays using established surgical procedures [7], [9]. The arrays consisted of four 50 μm-wide thin-film silicon shanks separated by 200 μm. Each shank had four iridium microelectrodes (703 μm^2 site area) with 200 μm spacing between sites. In two of the rats, an array with activated iridium sites (described below) was implanted into the left primary auditory cortex [21] and an array with unactivated (native) iridium sites was implanted in the forelimb region of the rat's primary motor cortex [22]. The remaining six rats received either one or two arrays with native iridium sites in the forelimb region of primary motor cortex. In seven of the rats the rejuvenation protocol began at least three weeks (ranging from 26 to 97 d) after implantation, during which time the normal tissue reactive response is likely

0018-9294/$20.00 © 2006 IEEE

to stabilize [12]. In the remaining rat, the protocol began nine days postimplant. All data were combined for subsequent statistical analysis. The experimental procedures complied with the guidelines for the care and use of laboratory animals and were approved by the University of Michigan Committee on Use and Care of Animals.

The rejuvenation protocol was an *in vivo* procedure used on both native and activated iridium sites. The rejuvenation voltage was a 4 s duration, 1.5-V DC signal applied to an electrode site relative to a 316SS-grade stainless steel bone screw (electrode site positive). The current induced between the electrode site and the bone screw was sampled at 1 Hz. Control experiments were conducted by applying the rejuvenation protocol to electrodes immersed in phosphate-buffered saline referenced to a stainless-steel 316SS-grade electrode.

B. Neural Recordings

Extracellular recordings were obtained immediately before and after the rejuvenation protocol in order to evaluate the effects on the extracellular recording of action potentials. The recordings were made with a Multichannel Acquisition Processor (MAP) simultaneously for 16 channels (Plexon Inc, Denison, TX). The data were sampled at 40 kHz and band-pass filtered from 450–5000 Hz. Recorded data sets were typically 30 s in duration and repeated two to six times a day (as described below). Recordings were referenced differentially to a channel on the array with no clear unit activity. This was necessary to eliminate electrical artifact due to muscle movements within the recordings made prerejuvenation. The amplification of individual channels was adjusted between 1000 and 32 000 to access maximal dynamic range of the recording system. Single channels were selectively monitored on an oscilloscope and audio monitor. The subjects were awake, typically sitting quietly in an electrically and acoustically shielded chamber during the recording sessions.

The electrophysiological data were analyzed offline using custom software in Matlab (Mathworks, Natick, MA). An objective measure of signal quality was developed using wavelet analysis to estimate noise amplitude, signal amplitude, and the signal-to-noise ratio (SNR). The wavelet analysis has been described elsewhere [23]. Briefly, for each channel, a wavelet decomposition at level 4 was composed using a Symlet wavelet family. For each decomposition vector, the root-mean square (RMS) was calculated. Values in the decomposition vector that were less than three times the overall RMS level were considered subthreshold and the RMS of these values was tabulated as the estimate of the noise amplitude. The estimate of the signal amplitude within the decomposition vector was calculated as the RMS of the remaining values. The overall channel noise amplitude and signal amplitude was determined by calculating a modified RMS of all of the decomposition vectors, emphasizing the lower level nodes. The SNR ratio was then calculated as the ratio of the overall signal amplitude to the overall noise amplitude. Means were calculated from repeated measures taken both before and after rejuvenation for the noise, signal and SNR values.

C. Electrochemical Measurements

Electrochemical measurements were made with a two-electrode cell configuration using an Autolab potentiostat (PGSTAT12, Eco Chemie, Utrecht, The Netherlands) that includes a frequency response analyzer (Brinkmann, Westbury, NY). Individual iridium sites on the microelectrode array were the working electrodes and a stainless steel (316SS-grade) bone screw was the reference electrode for all electrochemical measurements. The measured electrochemical potential of the 316SS bone screw relative to a saturated calomel electrode in 0.1 M phosphate buffered saline (Fischer Scientific, Fair Lawn, NJ) was 0.026 V. The potentiostat system internally measured and zeroed the open circuit potential of the electrode site relative to the bone screw reference electrode before each measurement. Moreover, the 316SS grade reference electrode is corrosion resistant and provides stable peak potentials in cyclic voltammagrams, suggesting a stable reference potential *in vivo* [24]. In these experiments, peak potentials were stable throughout the implant duration.

While arrays implanted in the motor cortex had native iridium electrode sites, arrays implanted in the auditory cortex had electrode sites with layers of activated hydrous iridium oxide. Activation of selected iridium electrode sites used an established technique that involves applying a 1-Hz square wave with a 1-V positive (anodic) amplitude and $-0.85-\mathrm{V}$ (cathodic) amplitude, referenced to the stainless steel bone screw [25], [26]. The nominal duration of the activation waveform was 100 s to create site charge densities approximately 30 $\mathrm{mC/cm^2}$.

Two types of potentiostatic measurements were made prior to and immediately after rejuvenation sessions in order to assess reduction-oxidation reactions at the interface, charging of the double layer, and charge capacity (*Qcap*). Electrochemical impedance spectroscopy (EIS) measurements were made using a 25 mV RMS sine wave at 11 frequencies ranging logarithmically from 100 Hz to 10 kHz. Cyclic voltammetry (CV) measurements were made using a linearly sweeping voltage between -0.75 V and $+0.75$ V with a 1 V/s scan rate. *Qcap* was calculated by integrating the area of the cyclic voltammagram for the positive voltage scan.

D. Neural Interface Model

A lumped element, equivalent circuit model was used to analyze the effects of rejuvenation on components of the electrode-tissue interface (Fig. 1). The model was based on a previous model of the reactive tissue response to implanted microelectrode arrays [27], [28]. The model includes an iridium site component and a neural tissue component, with the latter determined by electrical characteristics of the reactive tissue response [29]. Microelectrode encapsulation is characterized, in part, by protein adsorption onto the electrode site and an adjacent layer of connective tissue [10] given by a sealing resistance (R_{en}). Adjacent to this layer is often a sheath of glial cells and other macrophages that form an equivalent circuit having a membrane capacitance $(C_m = 1 \times 10^{-6}\ \mu\mathrm{F/cm^2})$ and a membrane conductance $(1/R_m = g_m = 0.3\ \mathrm{S/cm^2})$ [30]. In the model, C_m and R_m are lumped together and represented by the membrane area scaling term, A_m. Rather than crossing the cellular

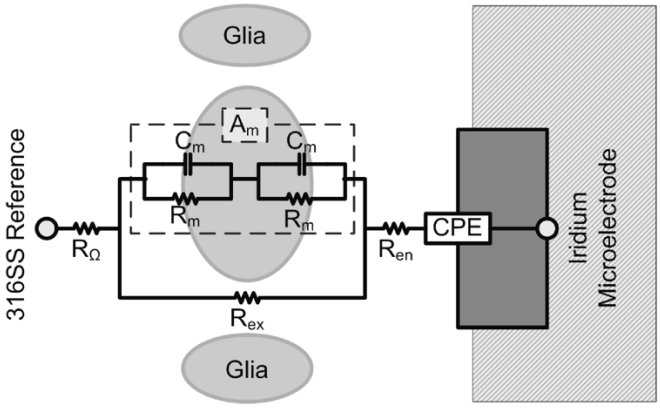

Fig. 1. Equivalent circuit model of the iridium microelectrode and surrounding neural tissue. Solid lines indicate electrical connections between the circuit elements. The circuit elements within the dotted line were lumped into the scaling term A_m. CPE: constant phase element; R_{en}: sealing resistance; A_m: membrane area scaling term; R_m: membrane resistance; C_m; membrane capacitance; R_{ex}: extracellular resistance; R_Ω: spreading resistance.

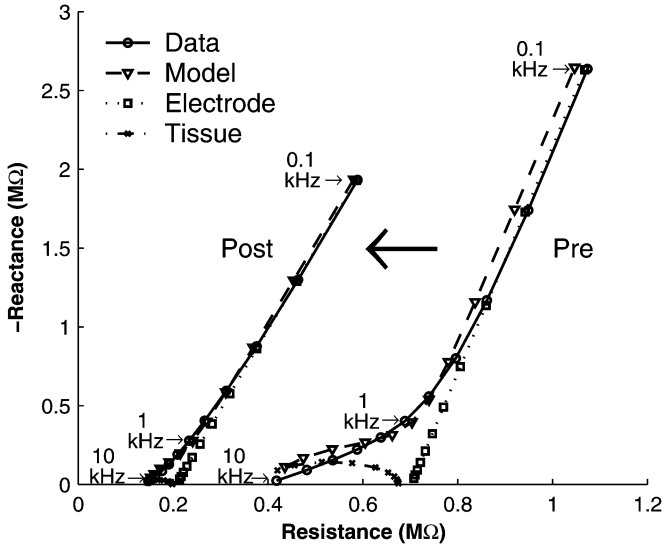

Fig. 2. An example of the neural interface model's goodness of fit (between the modeled impedance spectra and the measured impedance spectra) for a typical prerejuvenation and postrejuvenation set of complex impedance data points. The model values reflect the combined impedance of the entire model shown in Fig. 1. These values are then partitioned to reflect the contributions from the CPE (electrode) and the remaining elements (tissue). Three of the frequencies used to acquire the impedances are annotated.

membranes, current can flow in an extracellular domain represented by the resistance, R_{ex}. Thus, A_m reflects the ratio of the impedance of the cellular components near the electrode site to the impedance of the extracellular domain (R_{ex}). With the relatively large surface area of the bone screw, the spreading resistance (R_Ω) was estimated as less than 1 kΩ at all frequencies and assumed to be negligible. The measured shunt capacitance was < 10 pF and was subtracted from the complex impedance at each frequency. The measured resistance of the lead wires was $< 3\ \Omega$ and, thus, not included in the model.

A nonlinear regression algorithm was developed to estimate values of the circuit components in the model from the complex impedance spectroscopy measurements. The algorithm iteratively fit high- and low-frequency data points to their respective circuit paths in the model. Fitting of model parameters to the data involved minimizing the objective function J

$$J = \sum_{k=1}^{N} \frac{\left(Zre_k - \hat{Z}re_k\right)^2}{w_k^2} + \sum_{k=1}^{N} \frac{\left(Zj_k - \hat{Z}j_k\right)^2}{w_k^2} \quad (1)$$

where k reflects a particular impedance measurement frequency, N is the number of impedance measurement frequencies, Zre is the real component of the impedance measurement, Zj is the imaginary component of the impedance measurement, and w is a weight given by the impedance magnitude $|Z|$. Incorporating weights within the function is important to prevent biasing J to the low-frequency data. Model estimations that did not fit a $0.95R^2$ measure were discarded. Fig. 2 shows a typical fit of the model to the complex impedance spectroscopy data, as well as the individual electrode and tissue contributions to the model data.

The low-frequency pathway is the current pathway through three circuit components: the electrode, R_{en}, and R_{ex}. The electrode component, Z_{CPE}, was modeled with a constant phase element (CPE) [see (2)], with an electrode impedance scaling factor (K) and a phase term (α) defined over $0 \leq \alpha \leq 1$

$$Z_{\mathrm{CPE}} = \frac{K}{(j\omega)^\alpha}. \quad (2)$$

The process involved first fitting the two lowest frequency measurements with a line in the complex impedance space (resistance versus reactance). The slope of this linear fit was used to determine α [see (3)]. The CPE is sufficient to describe the nonideal double-layer capacitance behavior of native iridium [31]. The other two circuit elements in the low-frequency pathway (R_{en} and R_{ex}) are estimated from the x-intercept of this linear fit. R_{en} and R_{ex} are used to calculate the electrode impedance scaling factor, K [see (4)] using the real (Z_{re}) and imaginary (Z_j) components of the impedance measurements

$$\alpha = \frac{2}{\pi}\arctan(\mathrm{slope}) \quad (3)$$

$$K = \frac{Z_{re} - j * Z_j - (R_{en} + R_{ex})}{(j\omega)^{-\alpha}}. \quad (4)$$

Given estimates of K, α. R_{en}, and R_{ex}, the tissue component, A_m, is calculated based on high-frequency data points in the impedance spectrum. The objective function, J [see (1)] is then calculated. Subsequent iterations are conducted to estimate the R_{en}, R_{ex}, and A_m values that minimize J.

For activated iridium sites, the electrode impedance (Z_{AIr}) was modeled [see (5)] with an additional parallel capacitance (C_{ox}) and serial resistance (R_{ox}) with respect to the CPE following Weiland *et al.* [24]. These two parameters were estimated from *in vitro* measurements prior to implanting the electrode array in order to differentiate high-frequency contributions between the activated site and the neural tissue

$$Z_{\mathrm{AIr}} = \frac{R_{\mathrm{ox}} + Z_{\mathrm{CPE}}}{1 + j\omega C_{\mathrm{ox}}(R_{\mathrm{ox}} + Z_{\mathrm{CPE}})}. \quad (5)$$

III. Results

All animals had been implanted for ≥ 1 week (ranging from 7 to 97 d) and had little discernable unit activity prior to rejuvenation. The rejuvenation voltage on a site (4 s, 1.5 V) resulted in small

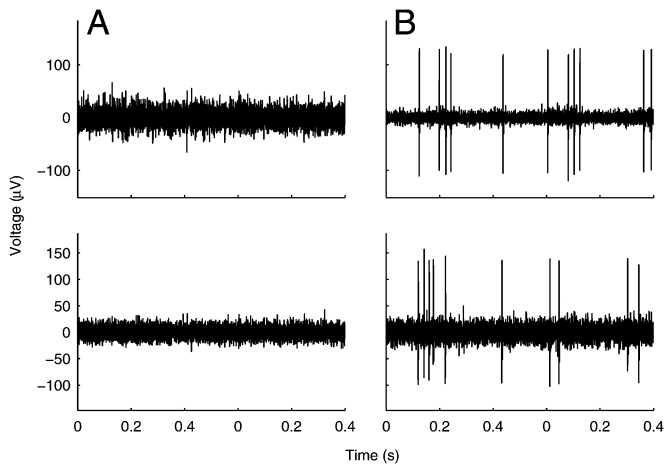

Fig. 3. A 1 s example of the most extreme effects of rejuvenation on the recording quality. (A) Prerejuvenation recordings from two electrodes with 3.74 and 3.37 SNR respectively. (B) Postrejuvenation recordings on these electrodes increased in SNR to 11.32 and 6.98 respectively.

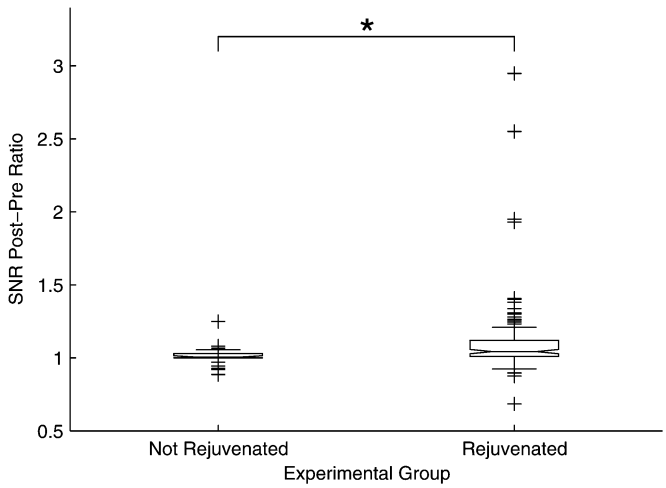

Fig. 4. Box and whisker plot showing the ratio of SNR postrejuvenation to the SNR prerejuvenation. Nearby electrodes not rejuvenated did not show a significant trend in the SNR ratio of postrejuvenation to prerejuvenation. SNR's increased after the rejuvenation voltage was applied in 114 of the 140 electrodes tested (asterisk indicates statistical significance of a t-test, $p < 0.001$).

currents flowing between the selected site and the bone screw reference (typically less than 300 nA, measured at 1 Hz). The current increased exponentially with a time constant of 0.4 s.

A. Voltage Pulse Effects on Neural Recordings

The rejuvenation voltage pulse caused a large increase in the SNR for a subset of the tested electrode sites (Fig. 3). On average, over all sites that were tested the SNR increased significantly from 3.63 to 4.00 a 10.4% increase ($n = 140, p < 0.001$, paired t-test). In 114/140 (81.4%) of the electrodes, the SNR increased above the prerejuvenation level (Fig. 4). In 42/140 (30.0%) of the electrodes the SNR increased more than 10%. In some cases readily discriminated single units were present postrejuvenation when no units were discriminable before rejuvenation, which resulted in the reported large increases in the SNR. This was the case for the maximum SNR increase from 3.74 to 11.32 a 194.8% increase, as illustrated in Fig. 3. The SNR for electrode sites on the arrays that were not rejuvenated did not significantly change from the prerejuvenation levels ($n = 28, p = 0.19$, paired t-test).

SNR increases for most electrodes were primarily attributed to a reduction in the noise recorded on the electrode. In 121/140 (86.4%) of the electrodes sites, the noise decreased postrejuvenation. Overall, the mean noise changed from 12.10 μV to 9.98 μV, a 17.5% decrease ($n = 140, p < 0.001$, paired t-test). The mean signal amplitude also decreased although by a smaller percentage. Rejuvenation caused a reduction in mean signal amplitude 44.11 μV to 40.28 μV, an 8.7% decrease ($n = 140$, $p < 0.001$, paired t-test).

B. Voltage Pulse Effects on Site Impedances in Vivo

Rejuvenation resulted in instantaneous drops in 1-kHz site impedances. For the native iridium implanted sites, initial 1-kHz site impedances were 2.39 MΩ and after rejuvenation were 525 kΩ, a 78% reduction ($n = 93$, paired t-test, $p < 0.001$). Similarly, site impedances for the activated iridium implanted sites were initially 1.23 MΩ and after rejuvenation were 309 kΩ, a 75% reduction ($n = 27$, paired t-test, $p < 0.001$).

Site impedance reductions were found to depend on the voltage used to provide the pulses. Via an implanted native iridium array, voltage pulses were stepped in 0.25-V increments for 4 s as shown in Fig. 5 (solid line) with 1-kHz site impedance measurements taken between each step. Site impedances decreased steadily after a $+0.75-$V pulse and plateaued after a $+1.50-$V pulse; thus, applying a $+1.75$ V pulse (not shown) did not cause a significant decrease in site impedance. Stepping the voltage pulse back to 0 V and beyond to -0.25 V did not produce a significant increase in impedance suggesting that rejuvenation caused a lasting change in the electrode-tissue interface. *In vitro* rejuvenation of native iridium microelectrodes caused a 43% drop in the 1-kHz impedance from 1.113 ± 0.064 MΩ to 637 ± 15 kΩ ($n = 10$, paired t-test $p < 0.001$) as shown in Fig. 5 (dotted line). Although these drops were significant, the *in vitro* normalized impedance decrease was significantly smaller than in the *in vivo* arrays. Further, for native iridium rejuvenated *in vitro*, the microelectrode site impedances dropped sharply at $+1.5$ V, whereas the *in vivo* arrays showed a more gradual fall-off above $+0.75$ V.

The four-second duration of the anodic pulse used in this study had been explored previously and shown effective at improving unit recordings [32]. We also explored alternative pulse durations ranging from 2 to 5 s. Longer rejuvenation durations (2 to 5 s) resulted in higher charge injections (9.2 nC to 465.2 nC); however, little effect of duration was seen in the value of the change in 1-kHz impedances or in neural interface parameters.

C. Voltage Pulse Effects on Neural Interface Model Parameters

Through the iterative algorithm, components in the neural interface model were estimated from the complex impedance spectroscopy data before and after rejuvenation (Fig. 6). Prior to rejuvenation, resistive circuit elements dominated the interface impedance within the model (M); however, after rejuvenation, the interface resistance decreased on average 578 kΩ in comparison to an average drop of 211 kΩ in interface reactance. This

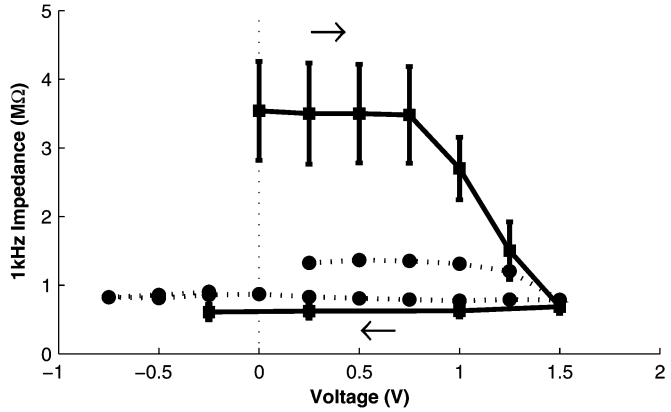

Fig. 5. Normalized 1-kHz impedances of *in vivo* (solid line) and *in vitro* (dotted line) native iridium sites as the voltage pulse was increased from 0 V to 1.5 V and subsequently decreased back to -0.25 V. Rejuvenation voltages between 1 and 1.5 V caused long-term decreases in the 1-kHz impedance. Error bars represent the standard error of measures taken for 10 sites in one subject (*in vivo*) or 17 sites (*in vitro*).

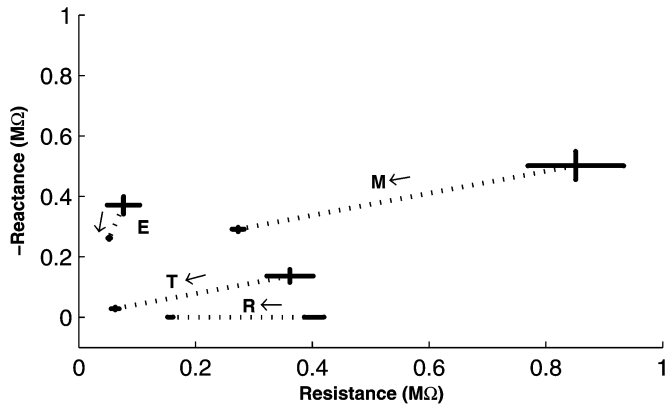

Fig. 6. Nyquist plot of average 1-kHz impedance of the entire circuit model (M) and contributions from the electrode component (E), the tissue component (T), and the encapsulated resistance (R). Each point is shown prior to and after rejuvenation, following the arrows. Each component demonstrated different degrees of rejuvenation-induced impedance drops. The error bars represent the standard error of the measured data.

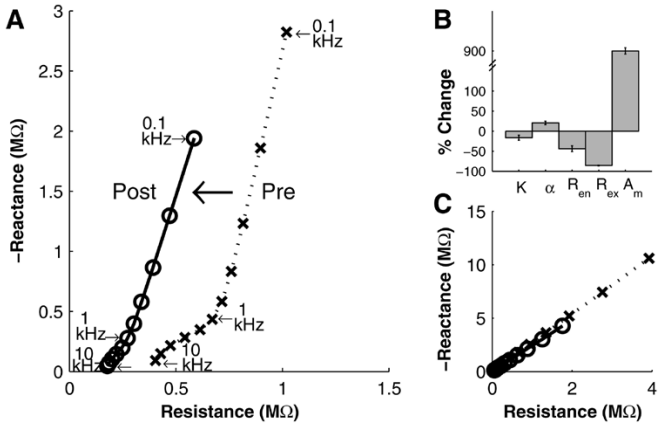

Fig. 7. Complex impedance spectra and subsequent model parameter changes of representative electrode sites prerejuvenation and postrejuvenation. (A) Impedance spectra from one site treated with *in vivo* rejuvenation show a significant impedance shift from prerejuvenated values (dotted line) to postrejuvenated values (solid line). (B) The individual component parameters from the model fitting routine applied to the data in (A) show significant changes due to *in vivo* rejuvenation. These changes were dominated by the tissue components of the model (R_{en}, R_{ex}, and A_m). (C) Impedance spectra from sites rejuvenated *in vitro* show smaller changes from prerejuvenation (dotted line) to postrejuvenation (solid line). *In vitro* rejuvenation resulted in smaller gain (K) changes compared to the *in vivo* results and show little change in the phase term (α).

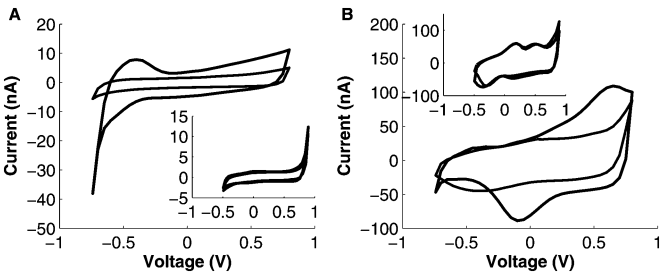

Fig. 8. Cyclic voltammetry results *in vivo* and *in vitro* rejuvenation. (A) Average of 16 *native* iridium sites before (gray line) and after (solid line) *in vivo* rejuvenation (inset: *in vitro*). (B) Average of 16 *activated* sites before and after *in vivo* rejuvenation (inset: *in vitro*).

resulted in an equal contribution of both types of impedances to the total interface impedance. The electrode component (E) impedance on average decreased primarily along the reactance axis, by an average of 109 kΩ, with only a 24 kΩ drop along the resistance axis. The tissue component (T) impedance decreased in terms of both resistance 299 kΩ and reactance 107 kΩ. A similarly large resistive decrease was evident in the encapsulated resistance component (R), dropping by 246 kΩ on average.

These general trends were analyzed further for native iridium sites to determine the electrode components, K and α. Representative complex impedance spectra for *in vivo* rejuvenation and *in vitro* rejuvenation are shown in Fig. 7(a) and (c) respectively. For *in vivo* and *in vitro* tests the electrode impedance scaling factor (K) decreased by 16.5% ($n = 73$, paired t-test, $p < 0.05$) and by 62.1%, ($n = 16$, paired t-test, $p < 0.05$) respectively. Overall, α increased for the *in vivo* tests by 11.9% ($n = 73$, paired t-test, $p < 0.001$) and there was not a significant change in the phase term in the *in vitro* tests.

The model consists of three cellular components, R_{ex}, A_m, and R_{en}. The two cellular tissue components, R_{ex} and A_m, both changed dramatically after rejuvenation. Representative values from one subject indicating the effect of rejuvenation on the fitted model parameters are shown in Fig. 7(b). Overall, the normalized value of R_{ex} for rejuvenated sites decreased by $86\pm1\%$ ($n = 73$, paired t-test, $p < 0.001$). The normalized value of R_{ex} for adjacent nonrejuvenated sites did not demonstrate a significant change ($n = 18$, paired t-test, $p = 0.508$, not shown). The normalized values for A_m on rejuvenated sites increased by $954 \pm 75\%$ ($n = 73$, t-test, $p < 0.001$). Again, the adjacent nonrejuvenated sites did not show a significant change ($n = 18$, t-test, $p = 0.644$, not shown). In contrast to the cellular components, the values for encapsulation resistance R_{en} decreased for both rejuvenated sites by $44 \pm 7\%$ ($n = 73$, t-test, $p < 0.001$) and for nonrejuvenated sites $31\pm5\%$ ($n = 18$, t-test, $p < 0.001$, not shown).

D. Voltage Pulse Effects on Electrode Charge Capacity

For *in vivo* rejuvenation, native iridium *Qcap* increased from 0.48 $\mathrm{mC/cm^2}$ to 1.70 $\mathrm{mC/cm^2}$ ($n = 16$, paired t-test, $p < 0.001$), and for previously activated iridium electrodes, from 6.37 $\mathrm{mC/cm^2}$ to 10.63 $\mathrm{mC/cm^2}$ ($n = 14$, paired t-test, $p < 0.001$) (Fig. 8). Fig. 8(a) shows that for the native iridium sites,

rejuvenation caused increased charge capacities for both oxidation and reduction voltages. In addition, the H_2 generation point shifted toward a more positive voltage, while a broad peak developed at negative voltages. *In vitro* rejuvenation had no affect on the cyclic voltammagram as shown in the inset. For activated iridium sites, rejuvenation similarly shifted, but also amplified, the oxidation and reduction peaks as shown in Fig. 8(b). Once again, upon applying the same protocol to *in vitro* arrays, the cyclic voltammagram waveforms did not change significantly after rejuvenation as shown in the inset. *In vitro* experiments did show that there was a slight change of $-0.124\,\mathrm{V}$ in the open circuit potential of the 316SS bone screw postrejuvenation (relative to a saturated calomel electrode). However, this was corrected for in the PGSTAT12 potentiostat by measuring the open circuit potential before every applied potential, ensuring that the potentials delivered for cyclic voltammetry were correct.

IV. Discussion

The present results demonstrate several effects of rejuvenation potentials on chronically implanted microelectrodes in the brain. First, there was an immediate impedance decrease measured at 1 kHz. Across the spectrum reported in this study, the impedance drop was complex in nature, but the main effect was the near elimination of the dominating resistive element that developed with the lifetime of the implant. Second, the SNR of the electrophysiological recordings obtained with the microelectrodes increased for the majority of the sites. This SNR increase was mainly due to a decrease in the magnitude of the noise recorded at the sites and resulted in clear action potential identification in some cases.

It has been shown in the literature that during the period post implant 1-kHz impedances generally rise and then stabilize with the lifetime of the chronically implanted electrodes [1]. Additionally, impedance spectroscopy has revealed that the complex impedance increase is due to both resistive and capacitive increases, and is highly correlated with the local immune response as determined by immunohistochemical markers [28]. Our prerejuvenation values support these studies, with 1-kHz impedance values elevated considerably above their preimplant values. Furthermore, the complex impedance spectra reported in this study indicate that both capacitive and resistive elements contribute to this increase, implicating a normal immune response around the electrode shanks.

Rejuvenation voltages applied to the microelectrode sites immediately decreased the microelectrode 1-kHz impedances to values comparable to those measured immediately postimplant. These impedance changes were voltage dependent with the largest changes occurring at 1.5 V versus the reference electrode. It has been shown in the literature that a single monolayer of anodic hydrous oxide is produced at the upper limits of a single cycle between potentials [33], [34]. The build-up of this layer is consistent with the initial anodic pulse during activation of iridium microelectrodes [24]. However, the magnitude of the increase of the storage capacity postrejuvenation in the cyclic voltammetry data cannot be explained completely by a single monolayer of anodic hydrous oxide. Thus, by applying an anodic pulse, the formation of a hydrous oxide monolayer may effectively remove ("clean-off") cellular and acellular debris that has formed proximal to the electrode site.

This "cleaning" of the microelectrode surface is supported by the changes in the model parameters. The largest changes were found for A_m and R_{ex}, implicating the cellular aspects of the model. These cellular model parameters were not affected for nearby sites that were not rejuvenated. There was also a significant change in the acellular model component R_{en}, and interestingly, the model parameter R_{en} decreased for both rejuvenated and nonrejuvenated sites. This suggests a change in the tissue resistance at distances not adjacent to the rejuvenated sites.

The most direct electrophysiological consequence of the changes at the electrode-tissue interface was a decrease in the noise of the recorded signal. Due to the decrease in the denominator of the SNR, it follows that the SNR of greater than 80% of the sites tested increased postrejuvenation. Often, although not always, this SNR increase manifested as clearly discriminable single neurons or multi-unit clusters. Whether these neurons were present and firing but could not be detected, or they were evoked from a silent state to begin to produce action potentials is still unknown. In the few cases where discriminable single neurons or multi-unit clusters were detectable prerejuvenation, the rejuvenation current did not appear to affect these cells adversely. Both the action potential waveshapes and the rate of action potential generation of these nearby neurons appeared unaffected by the nanoampere scale current utilized in the rejuvenation procedure. The 20% of the sites in which the SNR did not increase postrejuvenation were thought to have no nearby neuronal activity. Cases where the signal amplitude decreased, but the SNR increased were attributed to a reduction of the overall impedance between the electrode site and the reference, reducing the potentials generated by the membrane currents. This would also reduce the thermal noise of the recordings due to a reduction in the real component of the model impedance over the recording frequency band-pass.

All recordings in this study utilized differential recording in order to remove electrical artifacts due to movement. It should be noted that the differential recording procedure will artificially inflate the calculation of the noise level due to uncorrelated noise on the working and reference electrode. However, by increasing the noise level the effects of the rejuvenation would be seemingly diminished. Thus, the effects reported in this study are a conservative estimate of the effects of rejuvenation.

Several limitations of the model were considered during development. The ability of the model to adequately fit all of the data across the test situations implemented was a main design criterion. The main reason for poor model fit was too few data points at the low frequencies in order to determine the electrode components (K and α). In the results of this study only a few impedance spectra of site data were neglected from further analysis due to a poor model fit ($R^2 < 0.95$). Another limitation of the model, due to its lumped circuit implementation, is in its spatial resolution. Our model assumes homogeneous layers of neural tissue surrounding each implant site, disregarding variations within the neuropil surrounding the microelectrode site. However, a finite element model has demonstrated that 90% of the impedance is within 250 $\mu\mathrm{m}$ of the microelectrode site and 50% of the impedance within 30 $\mu\mathrm{m}$ [28].

In order to model the activated iridium sites, an additional capacitance (C_{ox}) in parallel to the CPE and a resistance (R_{ox}) was used. These values were assumed to be stable *in vivo* in the period following implantation. There are several arguments that validate this assumption. First, *in vitro* experiments demonstrated little change over time in terms of cyclic voltammetry peaks, charge storage capacity, and impedance spectra. Second, of the 32 activated sites, the data gathered from these two probes proved to be similar to the remaining 108 sites with native iridium sites. However, to the best of our knowledge, a detailed study on whether activated iridium oxide properties change over time *in vivo* has not been performed.

Further validation of the equivalent circuit model developed in this study will require predictions for different treatment situations followed by subsequent experiments to confirm these predictions. One application of the model is its use in assessing the long-term implications of rejuvenation on the microelectrode-neural tissue interface. Another application is to determine the feasibility of rejuvenation as a daily or weekly treatment for microelectrodes used for chronic neural recording.

The results of this study have direct implications for applications involving neurophysiological recording. The classic application example is in the use of extracellular recording for scientific research; however, the emerging neural engineering application of brain-machine interfaces requires a long-term neural interface [35], [36]. Rejuvenation may be a mechanism to improve the lifetime of chronically implanted neural recording devices.

V. Conclusion

This study investigated the underlying mechanisms of rejuvenation through an equivalent circuit model of the neural interface. Rejuvenation involved passing a small amount of current (typically 200 nA) over 4 s with a 1.5-V voltage pulse between an iridium microelectrode site and a stainless steel reference bone screw. Our findings indicate that rejuvenation caused a temporary enhancement to the electrode oxide conduction and a more substantial long-term change in the resistance of the encapsulated and extracellular spaces surrounding the microelectrode. This resulted in significantly better single and multi-unit recording from the microelectrode sites. This technique may be a useful intervention strategy to prolong the functional lifetime of chronically implanted microelectrode arrays.

Acknowledgment

The authors would like to thank J. Williams for discussion related to model development, and the Neural Engineering Laboratory for discussion relating to the manuscript. The authors would also like to thank J. Hetke and the CNCT for fabricating and assembling the probes.

References

[1] J. C. Williams, R. L. Rennaker, and D. R. Kipke, "Long-term neural recording characteristics of wire microelectrode arrays implanted in cerebral cortex," *Brain Res. Protoc.*, vol. 4, pp. 303–313, 1999.

[2] X. Liu, D. B. McCreery, R. R. Carter, L. A. Bullara, T. G. Yuen, and W. F. Agnew, "Stability of the interface between neural tissue and chronically implanted intracortical microelectrodes," *IEEE Trans. Rehabil. Eng.*, vol. 7, no. 3, pp. 315–326, Sep. 1999.

[3] M. A. L. Nicolelis, A. A. Ghazanfar, B. M. Faggin, S. Votaw, and L. M. Oliveira, "Reconstructing the engram: Simultaneous, multisite, many single neuron recordings," *Neuron.*, vol. 18, pp. 529–537.

[4] K. D. Wise, J. B. Angell, and A. Starr, "An integrated-circuit approach to extracellular microelectrodes," *IEEE Trans. Biomed. Eng.*, vol. BME-17, pp. 238–247, 1970.

[5] E. M. Maynard, C. T. Nordhausen, and R. A. Normann, "The Utah intracortical electrode array: A recording structure for potential brain-computer interfaces," *Electroencephalogr. Clin. Neurol.*, vol. 102, pp. 228–239, 1997.

[6] P. J. Rousche and R. A. Normann, "Chronic recording capability of the Utah intracortical electrode array in cat sensory cortex," *J. Neurosci. Meth.*, vol. 82, pp. 1–15, 1998.

[7] D. R. Kipke, R. J. Vetter, J. C. Williams, and J. F. Hetke, "Silicon-substrate intracortical microelectrode arrays for long-term recording of neuronal spike activity in cerebral cortex," *IEEE Trans. Neural Syst. Rehabil.*, vol. 11, no. 2, pp. 151–155, Jun. 2003.

[8] M. A. L. Nicolelis, D. F. Dimitrov, J. M. Carmena, R. C. G. Lehew, J. D. Kralik, and S. P. Wise, "Chronic, multisite, multielectrode recordings in macaque monkeys," *Proc. Natl. Acad. Sci. U.S.A*, vol. 100, pp. 11 041–11 046, 2003.

[9] R. J. Vetter, J. C. Williams, J. F. Hetke, E. A. Nunamaker, and D. R. Kipke, "Chronic neural recording using silicon-substrate microelectrode arrays implanted in cerebral cortex," *IEEE Trans. Biomed. Eng.*, vol. 51, no. 6, pp. 896–904, Jun. 2004.

[10] Y. T. Kim, R. W. Hitchcock, M. J. Bridge, and P. A. Tresco, "Chronic response of adult rat brain tissue to implants anchored to the skull," *Biomaterials*, vol. 25, pp. 2229–2237, 2004.

[11] D. H. Szarowski, M. D. Andersen, S. Retterer, A. J. Spence, M. Isaacson, H. G. Craighead, J. N. Turner, and W. Shain, "Brain responses to micromachined silicon devices," *Brain Res.*, vol. 983, pp. 23–35, 2003.

[12] J. N. Turner, W. Shain, D. H. Szarowski, M. Andersen, S. Martins, M. Isaacson, and H. G. Craighead, "Cerebral astrocyte response to micromachined silicon implants," *Exp. Neurol.*, vol. 156, pp. 33–49, 1999.

[13] S. S. Stensaas and L. J. Stensaas, "Histopathological evaluation of materials implanted in cerebral-cortex," *Acta Neuropathol.*, vol. 41, pp. 145–155, 1978.

[14] D. J. Edell, V. V. Toi, V. M. McNeil, and L. D. Clark, "Factors influencing the biocompatibility of insertable silicon microshafts in cerebral cortex," *IEEE Trans. Biomed. Eng.*, vol. 39, no. 6, pp. 635–643, Jun. 1992.

[15] P. J. Rousche and R. A. Normann, "A method for pneumatically inserting an array of penetrating electrodes into cortical tissue," *Ann. Biomed. Eng.*, vol. 20, pp. 413–422, 1992.

[16] X. Cui, V. A. Lee, Y. Raphael, J. A. Wiler, J. F. Hetke, D. J. Anderson, and D. C. Martin, "Surface modification of neural recording electrodes with conducting polymer/biomolecule blends," *J. Biomed. Mater. Res.*, vol. 56, pp. 261–272, 2001.

[17] W. Shain, L. Spataro, J. Dilgen, K. Haverstick, S. Retterer, M. Isaacson, M. Saltzman, and J. N. Turner, "Controlling cellular reactive responses around neural prosthetic devices using peripheral and local intervention strategies," *IEEE Trans. Neural Syst. Rehabil.*, vol. 11, no. 2, pp. 186–188, Jun. 2003.

[18] P. J. Rousche, D. S. Pellinen, D. P. Pivin, J. C. Williams, R. J. Vetter, and D. R. Kipke, "Flexible polyimide-based intracortical electrode arrays with bioactive capability," *IEEE Trans. Biomed. Eng.*, vol. 48, no. 3, pp. 361–371, Mar. 2001.

[19] K. D. Wise, "Second Quarterly Progress Report: Chronic Implantation of Passive Probes," Univ. Michigan, NIH Contract NIH-NINDS-NO1-N5-O-239.6, 1991.

[20] E. M. Schmidt, "Chronic neural recording with multi-contact silicon microprobes: Effects of electrode bias," *Soc. Neurosci. Abstr.*, vol. 20, pp. 982–982, 1994.

[21] S. L. Sally and J. B. Kelly, "Organization of auditory cortex in the albino rat: Sound frequency," *J. Neurophysiol.*, vol. 59, pp. 1627–1638, 1988.

[22] J. N. Sanes, S. Suner, and J. P. Donoghue, "Dynamic organization of primary motor cortex output to target muscles in adult rats. I. Long-term patterns of reorganization following motor or mixed peripheral nerve lesions," *Exp. Brain. Res.*, vol. 79, pp. 479–491, 1990.

[23] A. E. Snellings, J. W. Aldridge, and D. J. Anderson, "Use of multichannel recording electrodes and independent component analysis for isolating neural signals," *Soc. Neurosci. Abstr.*, vol. 29, 2003.

[24] J. D. Weiland and D. J. Anderson, "Chronic neural stimulation with thin-film, iridium oxide electrodes," *IEEE Trans. Biomed. Eng.*, vol. 47, no. 7, pp. 911–918, Jul. 2000.

[25] L. S. Robblee, J. L. Lefko, and S. B. Brummer, "Activated Ir—An electrode suitable for reversible charge injection in saline solution," *J. Electrochem. Soc.*, vol. 130, pp. 731–733, 1983.

[26] R. D. Meyer, S. E. Cogan, T. H. Nguyen, and R. D. Rauh, "Electrodeposited iridium oxide for neural stimulation and recording electrodes," *IEEE Trans. Neur. Sys. Reh.*, vol. 9, no. 1, pp. 2–11, Mar. 2001.
[27] J. C. Williams, D. R. Kipke, G. D. Smith, and W. Shain, "Modeling the complex electrical impedance spectral properties of the electrode-tissue interface," in *Neural Pros. Workshop Abstr.*, 2001.
[28] J. C. Williams, "Performance of chronic neural implants," Ph.D. dissertation, Arizona State Univ., Tempe, 2001.
[29] S. S. Stensaas and L. J. Stensaas, "Reaction of cerebral cortex to chronically implanted plastic needles," *Acta Neuropathol.*, vol. 35, pp. 187–203, 1976.
[30] J. R. Buitenweg, W. L. Rutten, W. P. Willems, and J. W. van Nieuwkasteele, "Measurement of sealing resistance of cell-electrode interfaces in neuronal cultures using impedance spectroscopy," *Med. Biol. Eng. Comput.*, vol. 36, pp. 630–637, 1998.
[31] E. T. McAdams, A. Lackermeier, J. A. Mclaughlin, D. Macken, and J. Jossinet, "The linear and nonlinear electrical-properties of the electrode-electrolyte interface," *Biosens. Bioelectron.*, vol. 10, pp. 67–74, 1995.
[32] W. J. Heetderks and E. M. Schmidt, private communication, 1997.
[33] P. G. Pickup and V. I. Birss, "A model for anodic hydrous oxide-growth at iridium," *J. Electroanal. Chem.*, vol. 220, pp. 83–100, 1987.
[34] B. E. Conway and J. Mozota, "Surface and bulk processes at oxidized iridium electrodes. 1. Monolayer stage and transition to reversible multilayer oxide film behavior," *Electrochim. Acta*, vol. 28, pp. 1–8, 1983.
[35] P. G. Patil, J. M. Carmena, M. A. Nicolelis, and D. A. Turner, "Ensemble recordings of human subcortical neurons as a source of motor control signals for a brain-machine interface," *Neurosurgery*, vol. 55, pp. 27–35, 2004.
[36] P. R. Kennedy, R. A. Bakay, M. M. Moore, K. Adams, and J. Goldwaithe, "Direct control of a computer from the human central nervous system," *IEEE Trans. Rehabil. Eng.*, vol. 8, no. 2, pp. 198–202, Jun. 2000.

Kevin J. Otto (M'03) received the B.S. degree in chemical engineering from Colorado State University, Fort Collins, in 1997 and the M.S. degree in bioengineering in 2002 and the Ph.D. degree in bioengineering in 2003 from Arizona State University, Tempe.

From 1997 to 2003, he was a Research Assistant in the Bioengineering Department, Arizona State University, where his work was in the areas of neural engineering and sensory neuroprostheses. From 2003 to 2004, he was a Research Fellow in the Department of Biomedical Engineering, University of Michigan, Ann Arbor, where his work focused on brain-machine interface systems and implantable devices. He is currently a Postdoctoral Fellow in the Central Systems Laboratory in the Kresge Hearing Research Institute in the Department of Otolaryngology at the University of Michigan. His research interests include neuroprostheses, systems neuroscience, and neurotechnologies.

Matthew D. Johnson (M'03) received the S.B. degree in engineering sciences from Harvard University, New Haven, CT, in 2002 and the M.S. degree in biomedical engineering from the University of Michigan, Ann Arbor, in 2003. He is currently working toward the Ph.D. degree in biomedical engineering at the University of Michigan.

From 2000 to 2002, he was a Research Assistant in the Harvard BioControls Laboratory, where his work was in the area of telemetry and neural engineering. Since 2002, he is a Research Assistant in the Neural Engineering Laboratory at the University of Michigan. His research interests include the application of BioMEMS to detect neurochemicals *in vivo* and the evaluation of chronically implanted neural probe microsystems.

Daryl R. Kipke (S'87–M'90) received the B.Sc. degree in engineering science in 1985, the M.Sc. degree in bioengineering in 1986, the M.S.E. degree in electrical engineering in 1988, and the Ph.D. degree in bioengineering in 1991 from the University of Michigan, Ann Arbor.

From 1991 to 1992, he was a Research Associate in the Department of Bioengineering and the Institute for Sensory Research at Syracuse University, Syracuse, NY. In 1992, he joined the Bioengineering faculty at Arizona State University, Tempe. In 2001, he joined the faculty of the College of Engineering at the University of Michigan. He is currently an Associate Professor in the Departments of Biomedical Engineering and Electrical Engineering and Computer Science at Michigan and directs the Neural Engineering Laboratory (http://nelab.engin.umich.edu). His primary research interests are in the areas of BioMEMS for neural implants, neuroprostheses, systems neuroscience, functional neurosurgery, and neurotechnologies. He teaches in the areas of biomedical instrumentation and neural engineering.

Dr. Kipke is a Fellow of the American Institute of Medical and Biological Engineering (AIMBE).